



Published in final edited form as:

Science. 2022 January 21; 375(6578): eabl6251. doi:10.1126/science.abl6251.

Structural basis for continued antibody evasion by the SARS-CoV-2 receptor-binding domain

Katherine G. Nabel^{1,†}, Sarah A. Clark^{1,†}, Sundaresh Shankar^{1,†}, Junhua Pan^{1,†}, Lars E. Clark¹, Pan Yang¹, Adrian Coscia¹, Lindsay G.A. McKay², Haley H. Varnum¹, Vesna Brusic¹, Nicole V. Tolan³, Guohai Zhou⁴, Michaël Desjardins^{5,6}, Sarah E. Turbett^{7,8}, Sanjat Kanjilal^{5,9}, Amy C. Sherman⁵, Anand Dighe⁸, Regina C. LaRocque⁷, Edward T. Ryan^{7,10}, Casey Tylek¹¹, Joel F. Cohen-Solal¹¹, Anhdao T. Darcy¹¹, Davide Tavella¹¹, Anca Clabbers¹¹, Yao Fan¹¹, Anthony Griffiths², Ivan R. Correia¹¹, Jane Seagal¹¹, Lindsey R. Baden^{4,5,13}, Richelle C. Charles⁷, Jonathan Abraham^{1,5,12,13,*}

¹Department of Microbiology, Blavatnik Institute, Harvard Medical School; Boston, MA 02115, USA.

²Department of Microbiology and National Emerging Infectious Diseases Laboratories, Boston University School of Medicine; Boston, MA 02118, USA.

³Department of Pathology, Brigham and Women's Hospital; Boston, MA 02115, USA.

⁴Center for Clinical Investigation, Brigham and Women's Hospital; Boston, MA 02115, USA.

⁵Department of Medicine, Division of Infectious Diseases, Brigham and Women's Hospital; Boston, MA 02115, USA.

*Correspondence to: jonathan_abraham@hms.harvard.edu.

†These authors contributed equally to this work.

Author contributions:

Conceptualization: KGN, SAC, SS, JP, LEC, PY, AC, LGAM, NVT, MD, SET, SK, ACS, AD, CT, JFC, ATD, ATD, DT, AC, YF, AG, IRC, JS, LRB, RCC, JA

Methodology: KGN, SAC, SS, JP, LEC, PY, AC, LGAM, HHV, NVT, GZ, MD, SET, SK, ACS, AD, RCL, ETR, CT, JFC, ATD, DT, AC, YF, AG, IRC, JS, LRB, RC, JA

Investigation: KGN, SAC, SS, JP, LEC, PY, AC, LGAM, HHV, VB, NVT, SET, SK, MJ, ACS, CT, JFC, ATD, DT, AC, YF, AG, IRC, JS, LRB, RC, JA

Visualization: KGN, SAC, SS, JP, LEC, PY, AC, LGAM, HHV, NVT, GZ, MD, SET, SK, ACS, CT, JFC, ATD, DT, AC, YF, AG, IRC, JS, LRB, RCC, JA

Funding acquisition: RCL, ETR, RCC, JA

Project administration: KGN, SAC, SS, JP, NVT, MD, SET, SK, ACS, AG, IRC, JS, LRB, RCC, JA

Supervision: AD, JFC, YF, AG, IRC, JS, LRB, RCC, JA

Writing – original draft: JA

Writing – review & editing: KGN, SAC, SS, JP, LEC, AC, LGAM, HHV, GZ, MD, SET, SK, ACS, RCL, ETR, CT, JFC, ATD, DT, AC, YF, AG, IRC, JS, LRB, RCC, JA

Competing interests: SAC, LEC, and JA are inventors on a provisional application protecting various aspects of inventions described in this publication has been filed by the President and Fellows of Harvard University. S.E.T. receives monetary compensation from UpToDate. CT, JFC, ATD, DT, AC, YF, IRC, JS are AbbVie employees and may own AbbVie stock.

Data and materials availability: C1C-A3 antibody heavy chain and light chain variable region gene sequences have been deposited in GenBank under accession codes [OL621229](#) and [OL621230](#), respectively. Protein Data Bank (PDB) identification numbers for the day 146* RBD human ACE2 ectodomain complex, the unliganded C1C-A3 Fab, the C1C-A3 Fab SARS-CoV-2 spike protein ectodomain complex, and focused refinement of the C1C-A3 Fab/RBD region are 7SN0, 7SN1, 7SN3, and 7SN2, respectively. Electron Microscopy Database (EMDB) accession numbers for the C1C-A3 Fab SARS-CoV-2 spike protein ectodomain complex and focused refinement of the C1C-A3 Fab/RBD region are EMD-25210 and EMD-2509, respectively. All materials are available upon request.

⁶Department of Medicine, Division of Infectious Diseases, Centre Hospitalier de l'Université de Montréal; Montreal, QC H2X 0C1, Canada.

⁷Department of Medicine, Division of Infectious Diseases, Massachusetts General Hospital; Boston, MA 02114, USA.

⁸Department of Pathology, Massachusetts General Hospital; Boston, MA 02114, USA.

⁹Department of Population Medicine, Harvard Pilgrim Health Care Institute and Harvard Medical School; Boston, MA 02215, USA.

¹⁰Department of Immunology and Infectious Diseases, Harvard T.H. Chan School of Public Health; Boston, MA 02215, USA.

¹¹AbbVie Bioresearch Center, 100 Research Drive, Worcester, MA 01605, USA

¹²Broad Institute of Harvard and MIT; Cambridge, MA 02142, USA.

¹³Massachusetts Consortium on Pathogen Readiness; Boston, MA USA.

Abstract

Many studies have examined the impact of SARS-CoV-2 variants on neutralizing antibody activity after they have become dominant strains. Here, we evaluate the consequences of further viral evolution. We demonstrate mechanisms through which the SARS-CoV-2 receptor-binding domain (RBD) can tolerate large numbers of simultaneous antibody escape mutations and show that pseudotypes containing up to seven mutations, as opposed to the one to three found in previously studied variants of concern, are more resistant to neutralization by therapeutic antibodies and serum from vaccine recipients. We identify an antibody that binds the RBD core to neutralize pseudotypes for all tested variants but show that the RBD can acquire an N-linked glycan to escape neutralization. Our findings portend continued emergence of escape variants as SARS-CoV-2 adapts to humans.

One-Sentence Summary:

As it evades antibodies, the SARS-CoV-2 spike protein receptor-binding domain can acquire composite mutations and a glycan.

As SARS-CoV-2 continues to replicate in humans under selective pressure from natural and vaccine induced immunity, variants of concern (VOCs) with increased transmissibility or virulence continue to emerge (1). Through adaptive evolution, these variants acquire mutations in the spike protein receptor-binding domain (RBD) that binds the cellular receptor human angiotensin-converting enzyme 2 (ACE2) (1-3). Many of these mutations are within the RBD “receptor-binding motif” (RBM), a hypervariable loop that mediates most of the ACE2 contacts (2, 3). The RBD is the primary target of neutralizing antibodies in naturally acquired or vaccine-elicited humoral immunity (4, 5). The spike protein N-terminal domain (NTD) is also a target of neutralizing antibodies, and VOCs have NTD mutations including deletions at an antigenic supersite for neutralizing antibody binding (6, 7). The effects of spike protein mutations on immune responses (8-13) make it important to monitor viral variants.

While previously studied VOCs contain one to three RBD mutations that at times overlap (1), the potential for composite variants is being closely monitored. For example, the B.1.617.2 (Delta) variant can acquire the K417N_{RBD} mutation found in the B.1.351 (Beta) variant, generating the Delta AY.2 variant, for a total of three RBD mutations (Fig. 1A). Similarly, as shown in recently deposited sequences from samples collected in Angola, the Beta variant can acquire the L452R_{RBD} mutation found in the Delta and B.1.429/427 (Epsilon) variants, for a total of four RBD mutations (Fig. 1A and table S1). Further complicating matters, variant monitoring efforts are still under sampling viral evolution. For example, a virus recently sequenced from travelers returning from Tanzania contained a previously undocumented combination of RBD mutations (E484K_{RBD}, T478R_{RBD}, and R346K_{RBD}) with NTD deletions that would likely alter the spike protein antigenic surface and result in antibody escape (table S1).

Here, we investigate the structural plasticity of the SARS-CoV-2 spike protein RBD and its capacity to evade neutralizing antibodies.

Results

Structure of an evolved receptor-binding domain ACE2 complex

We previously generated two SARS-CoV-2 spike proteins that each contain six RBD changes that were detected during persistent infection of an immunocompromised individual infected with a SARS-CoV-2 strain containing the D614G_S mutation (14-16). This individual received treatment with REGN-COV2 (17, 18), but several of the RBD substitutions had occurred even prior to administration of this therapeutic antibody cocktail (14-16). Lentivirus pseudotypes bearing these spike proteins, denoted day 146* and day 152* (Fig. 1A and table S2), were refractory to neutralization by V_H3-53-heavy chain gene-derived neutralizing antibodies, a potent class of neutralizing antibodies that have been repeatedly isolated from convalescent donors (19-25). These pseudotypes were also resistant to neutralization by components of REGN-COV2 (17, 18) and by polyclonal immunoglobulins (IgG) purified from the serum of COVID-19 convalescent donors (14). Substitutions in the day 146* and day 152* spike proteins, noted in samples sequenced from this individual in the spring and summer of 2020, foreshadowed those in currently circulating VOCs at three positions: N501_{RBD}, E484_{RBD}, and T478_{RBD} (Fig. 1A). The day 146* and day 152* spike proteins also contain substitutions that are not in current dominant strains but could have serious effects if acquired. For example, the S494P_{RBD} substitution is a therapeutic antibody (LY-CoV555) escape mutation (26) that as of September 27th, 2021, was present in over 12,000 human-derived SARS-CoV-2 sequences on public research databases (GISAID) (27). Additionally, the Q493K_{RBD} mutation, which is found in over one hundred human-derived SARS-CoV-2 sequences as of September 27th, 2021, on GISAID, confers resistance to multiple therapeutic antibodies [REGN10933, CB6 (LY-CoV016), and LY-CoV555] and V_H3-53-gene-derived antibodies (14, 16, 17, 28).

To determine the impact of their combined mutations on human ACE2 binding, we generated recombinant RBDs for the day 146* and day 152* spike protein mutants. The affinity of the day 152* mutant monomeric RBD for monomeric ACE2 ectodomain was substantially lower (K_D of 2.4 μ M) than that of wild-type (Wuhan-Hu-1) RBD (54 nM,

consistent with other reports) (3, 29), suggesting that its mutations also compromise ACE2 binding (fig. S1 and table S3). For comparison, the affinity we measured of the SARS-CoV RBD for human ACE2 was 0.26 μM , about nine-fold higher than the affinity for the day 152* RBD (fig. S1 and table S3). The affinity of the day 152* RBD for ACE2 is comparable to that of the RBDs of some bat coronaviruses that are closely related to SARS-CoV-2 and bind human ACE2 (e.g., RaTG13 virus RBD affinity of 3.9 μM) (30). The day 146* RBD, however, had a similar affinity (K_D of 46 nM) for ACE2 as that of the Wuhan-Hu-1 SARS-CoV-2 RBD (fig. S1 and table S3).

We determined the X-ray crystal structure of the day 146* RBD bound to the human ACE2 ectodomain (Fig. 1B, fig. S2, and table S4). This structure is similar to previously determined structures of ACE2/SARS-CoV-2 RBD complexes (2, 3), except we observed contacts between two N-linked glycans on ACE2 (attached to N53_{ACE2} and N90_{ACE2}) and the RBD (fig. S3). Removing the N90_{ACE2} glycan, which interacts with the RBD in both copies of the crystal asymmetric unit (fig. S3), increased Wuhan-Hu-1 SARS-CoV-2 and day 146* RBD affinity for ACE2, although the effect was modest (fig. S1 and table S3). This finding is consistent with prior work implicating the N90_{ACE2} glycan, which is removed in a human polymorphism (T92I_{ACE2}), as a barrier to SARS-CoV-2 RBD binding to ACE2 (31, 32).

The N501Y_{RBD} substitution is found in multiple variants of concern (Fig. 1A); once it surfaced in the immunocompromised individual, it was retained at later time points (14-16). As also shown in a cryo-electron microscopy (cryo-EM) structure of the SARS-CoV-2 spike protein containing the N501Y_{RBD} substitution bound to ACE2 (33), the side chain of Y501_{RBD} interacts with Y41_{ACE2} and K353_{ACE2} with no significant structural change (Fig. 1, C and D). E484_{RBD} is a critical target of antibodies against SARS-CoV-2 and is mutated in several variants (12, 34, 35). In structures of Wuhan-Hu-1 SARS-CoV-2 RBD bound to ACE2, E484_{RBD} is near but does not directly contact the receptor (Fig. 1E). In the day 146* RBD/ACE2 complex structure, the K493_{RBD} sidechain reaches over the RBD surface to recruit the E484_{RBD} side chain to form a new salt bridge with K31_{ACE2} (Fig. 1F). The nearby Y489H_{RBD} mutation, which removes a polar contact with ACE2, better accommodates repositioning of E484_{RBD} because the histidine is smaller than the tyrosine sidechain and would avoid potential steric clashes with E484_{RBD} in this binding mode (Fig. 1, E and F). A second rotamer for residue H34_{ACE2} forms new RBD contacts to fill a gap created by the reorganization of local interactions (Fig. 1, E and F). This structural plasticity may explain how the RBD tolerates a surprisingly large number of mutations during intra-host evolution yet retains the ability to bind ACE2 tightly. It is also consistent with the large sequence divergence in the RBD residues that contact ACE2 among SARS-related coronaviruses that share this cellular receptor.

Neutralization escape of therapeutic antibodies

RBD-targeting antibodies can be categorized into classes based on whether they bind an overlapping footprint with ACE2 and recognize only an open or both an open and closed RBD on the spike protein trimer (36). CB6 (equivalent to LY-CoV016 or etesevimab) is a class 1, V_H3-66-derived antibody that blocks ACE2 binding and can only bind the RBD

when it is open, and LY-CoV555 (bamlanivimab) is a class 2 antibody that blocks ACE2 binding but can bind both open or closed RBDs (21, 37). LY-CoV016 and LY-CoV555 are used as a cocktail and bind epitopes that partially overlap on the RBM such that both cannot bind simultaneously (21, 37). REGN10933 is a class 1 antibody, and REGN10987 is a class 3 antibody that sterically blocks ACE2 binding but binds the RBM outside the main ACE2 binding site; both are used as a cocktail (REGN-COV2) (17, 18).

Structural plasticity at the RBD-ACE2 interface suggests that the RBD could tolerate many more mutations than found in current variants of concern. We next generated pseudotypes for spike protein variants that contain composite mutations. The Delta variant, which contains the L452R_{RBD} and T478K_{RBD} substitutions, has become a dominant strain across the globe (38). We generated pseudotype for the Delta AY.2 variant, which contains the K417N_{RBD} mutation that is usually found in the Beta variant, and a Delta variant containing the N501Y_{RBD}, E484K_{RBD}, and F490S_{RBD} mutations usually found in Beta, P.1 (Gamma), and C.37 (Lambda) variants (referred to here as “Delta +3”) (Fig. 1A, table S1, and table S2). The set of RBD mutations for the latter strain occurred in deposited sequences from samples collected in Turkey (table S1). We also generated pseudotypes in which we combined spike protein substitutions detected in the immunocompromised host with mutations found in the Beta variant, which we chose because this VOC is highly resistant to antibody neutralization (10, 12, 39). Starting with a day 146* spike protein sequence, which contains an NTD deletion, we incorporated either one (E484K_{RBD}) or two additional substitutions (E484K_{RBD} and K417N_{RBD}); these are referred to as receptor binding mutant-1 (RBM-1) and RBM-2, respectively (Fig. 1A and table S2). Additionally, starting with the Beta variant spike protein sequence, we generated a variant pseudotype that contains two additional mutations associated with immune evasion (L452R_{RBD} and N439K_{RBD}) (40, 41). This pseudotype is referred to as RBM-3 (Fig. 1A and table S2). An ACE2-Fc fusion protein neutralized RBM-1, RBM-2, and RBM-3 pseudotypes, suggesting that all entered cells by binding ACE2 (Fig. 2B and fig. S4A).

We tested the activity of therapeutic antibodies against Delta AY.2, Delta +3, RBM-1, RBM-2, RBM-3, and additional variant pseudotypes with known resistance profiles to serve as comparators in the same assay (Fig. 2, A and B, and fig. S4A). LY-CoV555 was the most impacted by escape mutations, followed by CB6 (from which LY-CoV016 is derived) (Fig. 2, A and B, and fig. S4A). The Q493K_{RBD} mutation conferred absolute resistance to LY-CoV555, generated eightyfold resistance to CB6, and also compromised REGN10933 activity, consistent with previous reports (Fig. 2, A and B, and fig. S4A) (14, 16, 17, 26). In addition to the expected loss of activity of LY-CoV555 and CB6 against Beta and Gamma variants (9, 11, 12, 42), LY-CoV555 and CB6 lost all activity against day 146*, day 152*, RBM-1, RBM-2, and RBM-3 pseudotypes (Fig. 2, A and B, and fig. S4A). While the Delta variant is known to resist neutralization by LY-CoV555 but retain sensitivity to neutralization by CB6/LY-CoV016 (38), Delta AY.2 pseudotype was resistant to both agents (Fig. 2, A and B, and fig. S4A). This is expected because CB6/LY-CoV016 is derived from a V_H3-66 antibody (21), and the additional mutation the Delta AY.2 variant contains with respect to Delta (K417N_{RBD}) confers resistance to CB6/LY-CoV016 and other members of the V_H3-53/V_H3-66 class of neutralizing antibodies (9, 14, 16, 26, 43). Delta +3 pseudotype, which despite containing six RBD mutations does not contain the K417N_{RBD} substitution,

only escaped neutralization by LY-CoV555 (Fig. 2, A and B, fig. S4A, and table S2). Although the distribution of LY-CoV016 and LY-CoV555 was paused in the United States in the summer of 2021 as the prevalence of Gamma and Beta VOCs increased, the distribution of this antibody cocktail has since been resumed with the rise of Delta as the predominant strain. However, our findings emphasize the importance of close monitoring of Delta AY.2 and of other Delta variants for acquisition of the K417N_{RBD} mutation.

Although REGN10933 lost substantial activity against the Beta variant, which is consistent with other reports (9, 12, 42), it still had an IC₅₀ value of less than 1 µg ml⁻¹ in our assays (Fig. 2, A and B, and fig. S4A). However, resistance markedly worsened with the day 146*, day 152*, RBM-1, RBM-2, and RBM-3 pseudotypes, with 800– to 1900–fold loss in neutralizing activity (IC₅₀ values ranging from 20 to 47 µg ml⁻¹). REGN10987 potently neutralized many of the variant pseudotypes we examined. While we observed expected resistance to REGN10987 neutralization by variants containing the N439K_{RBD} or the adjacent N440D_{RBD} substitutions (14, 16), we also observed some loss of activity against Epsilon and B.1.617.1 (Kappa), which was less expected because none of their substitutions fall within the REGN10987 RBD footprint (Fig. 1A and Movie 1). Other reports, nonetheless, have also noted varying degrees of modest in vitro resistance of Epsilon and Kappa variants to REGN10987 neutralization (39, 42). Notably, the day 146* and RBM-3 pseudotypes were the only ones to gain resistance to both antibodies in REGN-COV2 because they contain substitutions in the REGN10933 (e.g., Q493K_{RBD}, or E484K_{RBD} and K417N_{RBD}) and the REGN10987 binding sites (N439K_{RBD} or N440D_{RBD}) (Fig. 2, A and B, fig. S4A, and Movie 1) (14). We observed on GISAID instances of “day-146*-like” viruses that would be expected to resist neutralization by LY-CoV555, LY-CoV016, REGN10933, and REGN10987 because they contain the Q493K_{RBD} and N439K_{RBD} substitutions. One strain contains the N501Y_{RBD}, Q493K_{RBD}, and N439K_{RBD} mutations (sequenced once in South Africa), and the other contains the N501Y_{RBD}, Q493K_{RBD}, L452R_{RBD}, N439K_{RBD}, and N440F_{RBD} mutations (sequenced once in the United Kingdom) (table S1).

The broadly neutralizing antibody S309 (44), a class 3 antibody that binds the RBD but does not interfere with ACE2 binding, and from which the therapeutic antibody sotrovimab is derived, was active against all variants we tested (fig. S4A). However, we could not calculate reliable neutralization IC₅₀ values because of variable non-neutralizable pseudotype fractions (fig. S4A). The presence of a non-neutralizable fraction is unexplained but has been noted in other reports when human cells overexpressing ACE2, as opposed to African green monkey (Vero) target cells, were used to examine S309 neutralizing activity (45, 46).

Neutralization escape of mRNA vaccine recipient sera

Messenger RNA (mRNA)-based vaccines encoding the SARS-CoV-2 spike protein elicit robust neutralizing antibody responses (47-49). We directly compared immune evasion of the day 146*, day 152*, and RBM-2 pseudotypes to the B.1.1.7 (Alpha), Beta, and Gamma pseudotypes in sera obtained from individuals who had received a 2-dose series of an mRNA vaccine (BNT162b2 or mRNA-1273) (Fig. 2, C and D, and fig. S5). In addition to RBD

substitutions, day 146*, day 152*, RBM-1, and RBM-2 spike proteins all contain NTD deletions spanning residues 141-144, which are positioned near NTD mutations in Alpha, Beta, and Delta in a key antigenic supersite (table S2) (6, 7). As similar NTD deletions found in Alpha, Beta, and Delta prevent binding of some neutralizing antibodies (6, 7, 46), they would be expected to escape neutralization by some NTD-targeting antibodies in addition to escaping neutralization by RBD-targeting antibodies. After first immunization but prior to the second dose, we observed a loss in neutralizing activity for all variants, although the severity varied. Variants that contain any substitution at E484_{RBD}, combined with an NTD deletion (Beta, day 152*, and RBM-2), were more effective at evading antibody responses than variants that had an E484_{RBD} substitution without an NTD deletion (Gamma) or an NTD deletion but no E484_{RBD} substitution (day 146*) (Fig. 2, C and D, fig. S5, and table S2). These findings are consistent with the role of E484_{RBD} as a major driver in neutralization escape of polyclonal antibody responses to SARS-CoV-2 (35) and observations that Beta more robustly escapes antibody neutralization than Gamma (9, 13). They further suggest that variants that have an NTD supersite deletion and an E484_{RBD} substitution are the most concerning when it comes to resistance to polyclonal antibodies.

One quarter of sampled individuals had no detectable activity against the Beta and RBM-2 pseudotypes after a single immunization (Fig. 2, C and D). However, sampling at seven and twenty-eight days after the second immunization revealed detectable neutralizing activity against all variants in all vaccine recipients, including against the RBM-2 pseudotype, which contains seven RBD mutations (Fig. 2, C and D, and fig. S5). Thus, repeated administration of an mRNA vaccine encoding constructs of the SARS-CoV-2 spike protein used in current formulations may provide sufficient neutralizing antibody breadth and potency to yield baseline serum neutralizing activity against variants that are more extensively mutated than the current dominant strains.

Identification of SARS-CoV cross-reactive antibodies

The RBD is also the major target of neutralizing antibodies against SARS-CoV, which caused a small outbreak of viral pneumonia from 2003 to 2004, though with a much higher case fatality rate (50, 51). Polyclonal antibody responses against SARS-CoV-2 poorly cross-neutralize SARS-CoV (52, 53). To identify barriers that restrict neutralization breadth, we performed single memory B-cell sorting with the SARS-CoV spike protein to mine the memory B cell repertoire of a COVID-19 convalescent individual (“C1”). Polyclonal IgG from C1 plasma neutralized SARS-CoV-2 pseudotype but had weak activity against SARS-CoV pseudotype (fig. S6A). From C1 peripheral blood mononuclear cells (PBMCs), using a pre-fusion stabilized SARS-CoV spike protein (S2P) (54), we cloned 17 cross-reactive antibodies. Of these, eleven antibodies bound both SARS-CoV and SARS-CoV-2 spike protein in an ELISA (fig. S6C and table S5). Only the two RBD-binding antibodies, C1C-A3 (“A3”) and C1C-C6 (“C6”), neutralized SARS-CoV-2 pseudotypes in our assays (Figs. 2B and 3A, and fig. S6F). Despite binding to SARS-CoV spike protein and RBD by ELISA, A3 and C6 did not neutralize SARS-CoV pseudotype (fig. S6, F and G). We also included C1A-A6 (“A6”) in these assays, a SARS-CoV-2 neutralizing antibody we previously isolated from the C1 donor using pre-fusion stabilized SARS-CoV-2 S2P in single B-cell sorting experiments (14). Unlike A3 and C6, A6 neutralized SARS-CoV

pseudotypes (Figs. 2B and 3A, and fig. S6F). We determined Fab RBD binding affinities using biolayer interferometry (BLI) (fig. S7 and table S3) and confirmed A3 and A6 activity against infectious SARS-CoV-2 in a plaque reduction neutralization assay (fig. S4B).

A3 neutralized almost all SARS-CoV-2 variant pseudotypes with a neutralization IC_{50} value of less than $1 \mu\text{g ml}^{-1}$, including Beta, Gamma, Delta AY.2, Delta +3, RBM-1, RBM-2, and RBM-3 pseudotypes; the Epsilon variant was the only exception, with an IC_{50} value of $1.9 \mu\text{g ml}^{-1}$ (Fig. 2B and 3A, and fig. S4A). C6 and A6 also broadly neutralized variants but with higher baseline IC_{50} values, even against D614G_S pseudotypes (ranging from 2.0 to $11.4 \mu\text{g ml}^{-1}$) (Fig. 2B and 3A, and fig. S4A).

To determine where on the RBD A3, C6, and A6 bind, we carried out competition studies with C1A-B12 (14), a class 1 antibody; REGN10987 (17, 18) and S309 (44), two class 3 antibodies; and CR3022 (55), a class 4 antibody (Fig. 3B, fig. S8, and Movie 1). A3 competed with CR3022 and REGN10987 for RBD binding, C6 competed with CR3022, and C6 and A6 competed with each other (Fig. 3B and fig. S8). A6 did not compete with any of the other antibodies tested. Among A3, C6, and A6, only A3 competed with binding of an ACE2-Fc fusion protein, suggesting that A3 blocks cellular attachment.

Antibody C1C-A3 binds the conserved RBD core

We determined the 3.1 \AA cryo-EM structure of the A3 Fab bound to the SARS-CoV-2 spike protein ectodomain (Fig. 4A, figs. S9 and S10, and table S6). A3 binds the RBD core with the spike protein trapped in the three open RBD conformation (Fig. 4A). In agreement with competition assays (Fig. 3B), A3 interacts with RBD residues that overlap significantly with those of CR3022 (Fig. 3, C, D and E, and Movie 1). A3 is therefore a class 4 antibody, a class that includes CR3022, S2A4, S304, S2X35, H014, COVA1-16, S2X259, and DH1047 (4, 56-59) (Movie 1 and fig. S11). Although the A3 and S309 footprints on the RBD do not overlap and S309 (a class 3 antibody) can bind the closed spike protein trimer (44), both antibodies contact the N-linked glycan attached to N343_{RBD} but approach it from different faces (Fig. 3C and Movie 1).

The A3 Fab avoids the RBD-ACE2 interface, which contains the majority of key antibody escape mutations, but like other class 4 antibodies, nonetheless binds the RBD in a manner that would sterically interfere with ACE2 binding (Fig. 4, B-E, and fig. S11). Based on its epitope, in addition to retaining activity against all variants we tested, A3 would also have activity against emergent and pre-emergent SARS-CoV-2 variants; these include a virus sequenced from travelers from Tanzania that contains the E484K_{RBD}, T478R_{RBD}, and R346K_{RBD} mutations, and B.1.621 (Mu), a variant detected early in 2021 in Colombia that has since spread internationally and contains the E484K_{RBD}, N501Y_{RBD}, and R346K_{RBD} mutations (Fig. 1G, Fig. 4D, and table S1). The R346K_{RBD} mutation falls within the RBD core and is in the S309 binding site but is not within A3's footprint (Fig. 3, D and E, and Movie 1). However, S309 would likely retain activity against SARS-CoV-2 variants that contain the R346K_{RBD} mutation, as the residue that is at the position analogous to SARS-CoV R346_{RBD} is a lysine in SARS-CoV, and S309 neutralizes both SARS-CoV and SARS-CoV-2 (44, 60).

RBD core glycan addition drives neutralization escape

Despite A3's breadth against SARS-CoV-2 variant pseudotypes (Figs. 2B and 3A), A3 does not neutralize SARS-CoV pseudotype (fig. S6, F and G). The A3 epitope is highly conserved between SARS-CoV-2 and SARS-CoV; however, N370_{RBD} is a site of N-linked glycosylation in SARS-CoV (N357_{RBD} in SARS-CoV numbering) and in animal coronaviruses but not in SARS-CoV-2 (Fig. 5, A, B, C and F) (61). An N-linked glycan attached to SARS-CoV-2 N370_{RBD} would introduce steric clashes with the A3 antibody heavy and light chains (Fig. 5D). Furthermore, calculations of antibody accessible surface areas using molecular dynamic trajectories of a fully glycosylated SARS-CoV-2 spike protein with a modeled N370_{RBD} glycan suggest that its addition would restrict A3 epitope access and could also impact binding of other class 4 antibodies (fig. S12) (61, 62).

Partial occupancy of the glycan attached to SARS-CoV N357_{RBD} in recombinant protein preparations may explain how we observed spike protein and RBD binding but lack of SARS-CoV pseudotype neutralization (fig. S6, F and G). In surface plasmon resonance binding assays, A3 IgG bound tightly to the SARS-CoV RBD only when the RBD was enzymatically deglycosylated (fig. S13 and table S7). Consistent with the role of the SARS-CoV N357_{RBD} N-linked glycan as a barrier to A3 neutralization, introducing a substitution that would prevent its addition (T359A_{RBD}) sensitized SARS-CoV pseudotypes to A3 neutralization (IC₅₀ value of 5 $\mu\text{g ml}^{-1}$) (Fig. 2B and fig. S4A).

The A372S/T_{RBD} mutations, which would introduce an N-linked glycosylation motif and allow for modification of N370_{RBD} in the SARS-CoV-2 spike protein, are found in human-derived SARS-CoV-2 sequences (GISAID) (27), including on sequences for VOCs Alpha and Delta, without apparent geographic restriction (48 sequence counts as of October 10th, 2021, and detected in at least fourteen countries) (Fig. 5F and table S8). Although the mutations are currently rare, their presence in sequence databases suggest that SARS-CoV-2 strains containing these mutations can replicate in humans. To confirm that an N-linked glycan could be added to N370_{RBD}, we conducted glycan analysis on recombinant SARS-CoV-2 RBD containing the A372S_{RBD} substitution and observed 90% occupancy of an N-linked glycan at position N370_{RBD} (Fig. S13B)

Because acquisition of a putative N-linked glycan at N370_{RBD} was the most frequent on the Alpha variant at the time of our initial analysis, we generated an Alpha pseudotype that contains the A372T_{RBD} substitution (Alpha A372T). We tested the effect of this substitution on three class 4 antibodies: A3, the antibody we isolated here, S2A4, an antibody that does not cross-react with the SARS-CoV RBD (4) and COVA1-16, an antibody that has weak cross-neutralizing activity against SARS-CoV (57). The mutation resulted in eightfold resistance to A3 neutralization (IC₅₀ value of 1.1 $\mu\text{g ml}^{-1}$, as compared to 0.14 $\mu\text{g ml}^{-1}$ with Alpha pseudotype) and complete resistance to S2A4 neutralization (Fig. 2B, Fig. 3A, Fig 5, G and H, and fig. S4A). S2A4 and COVA1-16 neutralized variants with potency that was overall comparable to A3 in most cases (Fig. 2B, Fig. 3A, and fig. S4A). COVA1-16, probably because it has some activity against SARS-CoV (above the limit of detection in our assays but 29 $\mu\text{g ml}^{-1}$ as reported by Liu et al.) (57), retained activity against Alpha A372T pseudotype (Fig. 2B, Fig. 3A, Fig. 5H, fig. S4A). The Fab binding pose of certain class

4 antibodies, therefore, may allow them to avoid steric hindrance from an N-linked glycan attached to N370_{RBD} (S2X259 is an example of one such antibody) (Movie 1) (56).

Antibody C1C-A3 neutralizes a related coronavirus

Coronaviruses that circulate in animals and have spike protein RBDs that can bind human ACE2 are a continued threat. RaTG13 virus, which is closely related to SARS-CoV-2 phylogenetically, is an example of one such virus (63). The RaTG13 virus spike protein contains a threonine at RBD position 372, which would allow for N370_{RBD} glycosylation (Fig. 5F). Despite the presence of the N-linked glycan, A3 potentially neutralized RaTG13 virus pseudotype (neutralization IC₅₀ value of 21 ng ml⁻¹), suggesting that A3 neutralization breadth extends to pre-emergent coronaviruses that are closely related to SARS-CoV-2 (Fig. 5, G and H). Structural superposition reveals that the N370_{RBD} glycan on the RaTG13 RBD is positioned in a manner that may not block A3 epitope access but, rather, could interfere with binding of other antibodies that bind nearby epitopes on the RBD core (Fig. 5E).

Discussion

As variants containing composite mutations begin to emerge, continued SARS-CoV-2 immune evasion will remain a significant concern. We found that accumulation of large numbers of RBD mutations, which mimics accelerated spike protein evolution occurring in a persistently infected immunocompromised host (14-16), is facilitated by structural plasticity at the ACE2-RBD interface (Fig. 1, B-F). The severity of the phenotypes we observed in vitro suggest that further evolved variants will more adeptly escape therapeutic antibody neutralization than currently circulating variants of concern, with potential resistance to two-component antibody cocktails (Fig. 2, A and B).

After two mRNA vaccine immunizations and as early as seven days after the second dose, all mRNA vaccine recipients had detectable neutralizing activity against pseudotypes containing an NTD supersite deletion and RBDs with six to seven mutations (e.g., day 146*, day 152*, and RBM-2), with mean neutralization ID₅₀ values decreased by 2.3 to 6.1-fold (Fig. 2, C and D, and fig. S5). While the precise epitopes targeted by this residual vaccine-elicited serum neutralizing activity remain to be determined, we surmise that antibodies targeting the RBD core (e.g., those that bind away from the RBM), at least in part account for some of this activity. As the RBD is a major target of vaccine elicited and naturally acquired humoral immunity to SARS-CoV-2 (4, 5) and the RBM is a critical site of potent neutralizing antibody binding (19, 21-25, 64) that is the most antibody accessible and the least masked by glycan and conformational shielding (fig. S12), continued RBM evolution may guide antibody responses towards more conserved neutralizing epitopes on the RBD core.

We mined genome sequences in the GISAID database for substitutions that would introduce additional N-linked glycans onto the RBD. This analysis identified D364N_{RBD} as an additional mutation that would introduce a putative N-linked glycosylation site in a surface exposed loop in the footprint of some class 4 antibodies (Movie 1). The independent acquisition of N-linked glycosylation sites (through the A372S/T_{RBD} and D364N_{RBD}

substitutions) on the same surface of the RBD core, but not on other RBD sites, suggests that this region may be a target of immune selective pressure.

While glycan addition may allow neutralization escape, this change could come at a cost to viral fitness and infectivity. Indeed, the A1114G:T372A mutation that removed the glycan in the SARS-CoV-2 RBD appeared under selective pressure, and addition of the glycan decreases viral replication in human lung epithelial (Calu-3) cells by over sixty-fold (65). A recent molecular dynamics study suggests that introducing the glycan at N370_{RBD} in SARS-CoV-2 would favor the closed conformation with the N370_{RBD} glycan stabilizing the closed RBD structure on the trimeric spike protein (66). A lack of a glycan at position N370_{RBD}, therefore, may increase SARS-CoV-2 ACE2-binding and infectivity by favoring the open state, but may also make SARS-CoV-2 more vulnerable to neutralizing antibodies that can only bind the RBD in the open conformation.

Although addition of the N370_{RBD} glycan may be associated with a cost to viral fitness, should the selective immune pressure be significant at this site over a long enough time scale, this may also afford the virus an opportunity to acquire permissive secondary mutations during evolution that restore viral fitness, as is observed in influenza virus drug resistance (67). Such compensatory mutations would be ones that promote ACE2 binding and RBD opening; for example, the D614G_S mutation (68), which favors the open conformation, and the N501Y_{RBD} mutation, which introduces more favorable interactions with ACE2 (Fig. 1D).

As parts of the world continue to face waves of infection and mitigation strategies are relaxed, viral replication in human hosts under antibody selective pressure will continue to shape the antigenic landscape of the SARS-CoV-2 spike protein. With vigorous variant monitoring efforts underway to help design next-generation antibody-based therapeutics, and with mRNA- or DNA-based vaccines that can be updated to rapidly adapt to new variants, proactively examining the consequences of further viral evolution before the next highly antibody resistant strain emerges is of utmost importance.

Materials and methods summary

We isolated monoclonal antibodies from the blood of a COVID-19 convalescent individual using single B-cell sorting with prefusion stabilized SARS-CoV spike protein ectodomain as bait and using established protocols (14, 54). We obtained venous blood samples from healthy mRNA-1273 and BNT162b2 vaccine recipients. We produced recombinant glycoproteins and antibodies or Fabs in transiently transfected mammalian cells grown in suspension culture and purified these proteins using affinity-based methods. We used ELISAs to measure antibody binding and biolayer interferometry or surface plasmon resonance to determine kinetic parameters of binding. We packaged lentivirus pseudotypes by transient transfection of HEK293T cells as previously described (14). We used HEK293T cells expressing human ACE2 in pseudotype neutralization assays or Vero E6 cells and plaque reduction neutralization tests as previously described (14). We collected X-ray diffraction data on crystals of a day 146* SARS-CoV-2 RBD complex at the Advanced Photon Source (APS, Argonne, IL) NE-CAT beamline and used established procedures for

data processing, molecular replacement, atomic model building, and refinement (37, 69-73). We used mass spectrometry to perform glycopeptide analysis. After data collection on a Titan Krios cryo-electron microscope equipped with a Gatan K3 camera, we used single-particle cryo-EM to determine the structure of a prefusion stabilized SARS-CoV-2 spike protein ectodomain (7) complexed with C1C-A3 Fab complex using established procedures for image processing, atomic model building, and refinement (72-77).

Supplementary Material

Refer to Web version on PubMed Central for supplementary material.

Acknowledgments

This work is based upon research conducted at the Northeastern Collaborative Access Team (NE-CAT) beamlines, which are funded by the National Institute of General Medical Sciences from the National Institutes of Health (P30 GM124165). The Pilatus 6M detector on 24-ID-C beam line is funded by a NIH-ORIP HEI grant (S10 RR029205). This research used resources of the Advanced Photon Source, a U.S. Department of Energy (DOE) Office of Science User Facility operated for the DOE Office of Science by Argonne National Laboratory under Contract No. DE-AC02-06CH11357. We thank the staff at NE-CAT for assistance with X-ray data collection. Cryo-EM data were collected at the Harvard Cryo-Electron Microscopy Center for Structural Biology. We thank Harvard Cryo-EM Center staff members for assistance with cryo-EM data collection. We acknowledge support for COVID-19 related structural biology research at Harvard from the Nancy Lurie Marks Family Foundation. We thank B. Chen for providing a human ACE2 ectodomain expressing cell line, and H. Choe for providing cDNA encoding the SARS-CoV spike protein.

Funding:

This work was funded in part by the Massachusetts Consortium on Pathogen Readiness and China Evergrande Group (J.A.). J.A. was also supported by the Star-Friedman Award Challenge for Promising Scientific Research. L.R.B. is supported by the Harvard Clinical and Translational Science Center, from the National Center for Advancing Translational Science (1UL1TR002541-01); by Barbara and Amos Hostetter; and by the Chleck Family Foundation. S.E.T. receives grant support from the Centers for Disease Control and Prevention (U01CK000490). K.G.N., A.C., and H.H.V. are supported by Award Number T32GM007753 from the National Institute of General Medical Sciences. The content is solely the responsibility of the authors and does not necessarily represent the official views of the National Institute of General Medical Sciences or the National Institutes of Health.

References

1. Harvey WT et al. , SARS-CoV-2 variants, spike mutations and immune escape. *Nat Rev Microbiol* 19, 409–424 (2021). [PubMed: 34075212]
2. Lan J et al. , Structure of the SARS-CoV-2 spike receptor-binding domain bound to the ACE2 receptor. *Nature* 581, 215–220 (2020). [PubMed: 32225176]
3. Shang J et al. , Structural basis of receptor recognition by SARS-CoV-2. *Nature* 581, 221–224 (2020). [PubMed: 32225175]
4. Piccoli L et al. , Mapping neutralizing and immunodominant sites on the SARS-CoV-2 spike receptor-binding domain by structure-guided high-resolution serology. *Cell* 183, 1024–1042 e1021 (2020). [PubMed: 32991844]
5. Greaney AJ et al. , Antibodies elicited by mRNA-1273 vaccination bind more broadly to the receptor binding domain than do those from SARS-CoV-2 infection. *Sci Transl Med* 13, eabi9915 (2021). [PubMed: 34103407]
6. McCarthy KR et al. , Recurrent deletions in the SARS-CoV-2 spike glycoprotein drive antibody escape. *Science* 371, 1139–1142 (2021). [PubMed: 33536258]
7. McCallum M et al. , N-terminal domain antigenic mapping reveals a site of vulnerability for SARS-CoV-2. *Cell* 184, 2332–2347 e2316 (2021). [PubMed: 33761326]
8. Supasa P et al. , Reduced neutralization of SARS-CoV-2 B.1.1.7 variant by convalescent and vaccine sera. *Cell* 184, 2201–2211 e2207 (2021). [PubMed: 33743891]

9. Dejnirattisai W et al. , Antibody evasion by the P.1 strain of SARS-CoV-2. *Cell* 184, 2939–2954 e2939 (2021). [PubMed: 33852911]
10. Planas D et al. , Sensitivity of infectious SARS-CoV-2 B.1.1.7 and B.1.351 variants to neutralizing antibodies. *Nat Med* 27, 917–924 (2021). [PubMed: 33772244]
11. Wang P et al. , Increased resistance of SARS-CoV-2 variant P.1 to antibody neutralization. *Cell Host Microbe* 29, 747–751 e744 (2021). [PubMed: 33887205]
12. Wang P et al. , Antibody resistance of SARS-CoV-2 variants B.1.351 and B.1.1.7. *Nature* 593, 130–135 (2021). [PubMed: 33684923]
13. Garcia-Beltran WF et al. , Multiple SARS-CoV-2 variants escape neutralization by vaccine-induced humoral immunity. *Cell* 184, 2523 (2021). [PubMed: 33930298]
14. Clark SA et al. , SARS-CoV-2 evolution in an immunocompromised host reveals shared neutralization escape mechanisms. *Cell* 184, 2605–2617 e2618 (2021). [PubMed: 33831372]
15. Choi B et al. , Persistence and evolution of SARS-CoV-2 in an immunocompromised host. *N Engl J Med* 383, 2291–2293 (2020). [PubMed: 33176080]
16. Starr TN et al. , Prospective mapping of viral mutations that escape antibodies used to treat COVID-19. *Science* 371, 850–854 (2021). [PubMed: 33495308]
17. Baum A et al. , Antibody cocktail to SARS-CoV-2 spike protein prevents rapid mutational escape seen with individual antibodies. *Science*, 1014–1018 (2020).
18. Hansen J et al. , Studies in humanized mice and convalescent humans yield a SARS-CoV-2 antibody cocktail. *Science*, 1010–1014 (2020). [PubMed: 32540901]
19. Yuan M et al. , Structural basis of a shared antibody response to SARS-CoV-2. *Science*, 1119–1123 (2020). [PubMed: 32661058]
20. Rogers TF et al. , Isolation of potent SARS-CoV-2 neutralizing antibodies and protection from disease in a small animal model. *Science*, 956–963 (2020). [PubMed: 32540903]
21. Shi R et al. , A human neutralizing antibody targets the receptor-binding site of SARS-CoV-2. *Nature* 584, 120–124 (2020). [PubMed: 32454512]
22. Seydoux E et al. , Analysis of a SARS-CoV-2-infected individual reveals development of potent neutralizing antibodies with limited somatic mutation. *Immunity* 53, 98–105 e105 (2020). [PubMed: 32561270]
23. Robbiani DF et al. , Convergent antibody responses to SARS-CoV-2 in convalescent individuals. *Nature*, 437–442 (2020).
24. Du S et al. , Structurally resolved SARS-CoV-2 antibody shows high efficacy in severely infected hamsters and provides a potent cocktail pairing strategy. *Cell* 183, 1013–1023 e1013 (2020). [PubMed: 32970990]
25. Wu Y et al. , A noncompeting pair of human neutralizing antibodies block COVID-19 virus binding to its receptor ACE2. *Science*, 1274–1278 (2020).
26. Starr TN, Greaney AJ, Dingens AS, Bloom JD, Complete map of SARS-CoV-2 RBD mutations that escape the monoclonal antibody LY-CoV555 and its cocktail with LY-CoV016. *Cell Rep Med* 2, 100255 (2021). [PubMed: 33842902]
27. Elbe S, Buckland-Merrett G, Data, disease and diplomacy: GISAID's innovative contribution to global health. *Glob Chall* 1, 33–46 (2017). [PubMed: 31565258]
28. Weisblum Y et al. , Escape from neutralizing antibodies by SARS-CoV-2 spike protein variants. *Elife* 9, e61312 (2020). [PubMed: 33112236]
29. Wrapp D et al. , Cryo-EM structure of the 2019-nCoV spike in the prefusion conformation. *Science* 367, 1260–1263 (2020). [PubMed: 32075877]
30. Liu K et al. , Binding and molecular basis of the bat coronavirus RaTG13 virus to ACE2 in humans and other species. *Cell* 184, 3438–3451 e3410 (2021). [PubMed: 34139177]
31. Suryamohan K et al. , Human ACE2 receptor polymorphisms and altered susceptibility to SARS-CoV-2. *Commun Biol* 4, 475 (2021). [PubMed: 33846513]
32. Mehdipour AR, Hummer G, Dual nature of human ACE2 glycosylation in binding to SARS-CoV-2 spike. *Proc Natl Acad Sci U S A* 118, (2021).

33. Zhu X et al. , Cryo-electron microscopy structures of the N501Y SARS-CoV-2 spike protein in complex with ACE2 and 2 potent neutralizing antibodies. *PLoS Biol* 19, e3001237 (2021). [PubMed: 33914735]
34. Chen RE et al. , Resistance of SARS-CoV-2 variants to neutralization by monoclonal and serum-derived polyclonal antibodies. *Nat Med* 27, 717–726 (2021). [PubMed: 33664494]
35. Greaney AJ et al. , Comprehensive mapping of mutations in the SARS-CoV-2 receptor-binding domain that affect recognition by polyclonal human plasma antibodies. *Cell Host Microbe* 29, 463–476 e466 (2021). [PubMed: 33592168]
36. Barnes CO et al. , SARS-CoV-2 neutralizing antibody structures inform therapeutic strategies. *Nature* 588, 682–687 (2020). [PubMed: 33045718]
37. Jones BE et al. , The neutralizing antibody, LY-CoV555, protects against SARS-CoV-2 infection in nonhuman primates. *Sci Transl Med* 13, (2021).
38. Planas D et al. , Reduced sensitivity of SARS-CoV-2 variant Delta to antibody neutralization. *Nature* 596, 276–280 (2021). [PubMed: 34237773]
39. Chen RE et al. , In vivo monoclonal antibody efficacy against SARS-CoV-2 variant strains. *Nature* 596, 103–108 (2021). [PubMed: 34153975]
40. McCallum M et al. , SARS-CoV-2 immune evasion by the B.1.427/B.1.429 variant of concern. *Science* 373, 648–654 (2021). [PubMed: 34210893]
41. Thomson EC et al. , Circulating SARS-CoV-2 spike N439K variants maintain fitness while evading antibody-mediated immunity. *Cell* 184, 1171–1187 e1120 (2021). [PubMed: 33621484]
42. Wang L et al. , Ultrapotent antibodies against diverse and highly transmissible SARS-CoV-2 variants. *Science* 373, eabh1766 (2021). [PubMed: 34210892]
43. Yuan M et al. , Structural and functional ramifications of antigenic drift in recent SARS-CoV-2 variants. *Science* 373, 818–823 (2021). [PubMed: 34016740]
44. Pinto D et al. , Cross-neutralization of SARS-CoV-2 by a human monoclonal SARS-CoV antibody. *Nature* 583, 290–295 (2020). [PubMed: 32422645]
45. Rappazzo CG et al. , Broad and potent activity against SARS-like viruses by an engineered human monoclonal antibody. *Science* 371, 823–829 (2021). [PubMed: 33495307]
46. Liu C et al. , Reduced neutralization of SARS-CoV-2 B.1.617 by vaccine and convalescent serum. *Cell* 184, 4220–4236 e4213 (2021). [PubMed: 34242578]
47. Baden LR et al. , Efficacy and safety of the mRNA-1273 SARS-CoV-2 vaccine. *N Engl J Med* 384, 403–416 (2021). [PubMed: 33378609]
48. Polack FP et al. , Safety and efficacy of the BNT162b2 mRNA covid-19 vaccine. *N Engl J Med* 383, 2603–2615 (2020). [PubMed: 33301246]
49. Jackson LA et al. , An mRNA Vaccine against SARS-CoV-2 - Preliminary Report. *N Engl J Med* 383, 1920–1931 (2020). [PubMed: 32663912]
50. Ksiazek TG et al. , A novel coronavirus associated with severe acute respiratory syndrome. *N Engl J Med* 348, 1953–1966 (2003). [PubMed: 12690092]
51. Chen Z et al. , Recombinant modified vaccinia virus Ankara expressing the spike glycoprotein of severe acute respiratory syndrome coronavirus induces protective neutralizing antibodies primarily targeting the receptor binding region. *J Virol* 79, 2678–2688 (2005). [PubMed: 15708987]
52. Zhu Y et al. , Cross-reactive neutralization of SARS-CoV-2 by serum antibodies from recovered SARS patients and immunized animals. *Sci Adv* 6, eabc9999 (2020). [PubMed: 33036961]
53. Lv H et al. , Cross-reactive Antibody Response between SARS-CoV-2 and SARS-CoV Infections. *Cell Rep* 31, 107725 (2020).
54. Pallesen J et al. , Immunogenicity and structures of a rationally designed prefusion MERS-CoV spike antigen. *Proc Natl Acad Sci U S A* 114, E7348–E7357 (2017). [PubMed: 28807998]
55. Yuan M et al. , A highly conserved cryptic epitope in the receptor binding domains of SARS-CoV-2 and SARS-CoV. *Science* 368, 630–633 (2020). [PubMed: 32245784]
56. Tortorici MA et al. , Broad sarbecovirus neutralization by a human monoclonal antibody. *Nature* 597, 103–108 (2021). [PubMed: 34280951]
57. Liu H et al. , Cross-neutralization of a SARS-CoV-2 antibody to a functionally conserved site is mediated by avidity. *Immunity* 53, 1272–1280 e1275 (2020). [PubMed: 33242394]

58. Lv Z et al. , Structural basis for neutralization of SARS-CoV-2 and SARS-CoV by a potent therapeutic antibody. *Science* 369, 1505–1509 (2020). [PubMed: 32703908]
59. Li D et al. , In vitro and in vivo functions of SARS-CoV-2 infection-enhancing and neutralizing antibodies. *Cell* 184, 4203–4219 e4232 (2021). [PubMed: 34242577]
60. Starr TN et al. , SARS-CoV-2 RBD antibodies that maximize breadth and resistance to escape. *Nature* 597, 97–102 (2021). [PubMed: 34261126]
61. Watanabe Y et al. , Vulnerabilities in coronavirus glycan shields despite extensive glycosylation. *Nat Commun* 11, 2688 (2020). [PubMed: 32461612]
62. Grant OC, Montgomery D, Ito K, Woods RJ, Analysis of the SARS-CoV-2 spike protein glycan shield reveals implications for immune recognition. *Sci Rep* 10, 14991 (2020). [PubMed: 32929138]
63. Boni MF et al. , Evolutionary origins of the SARS-CoV-2 sarbecovirus lineage responsible for the COVID-19 pandemic. *Nat Microbiol* 5, 1408–1417 (2020). [PubMed: 32724171]
64. Hurlburt NK et al. , Structural basis for potent neutralization of SARS-CoV-2 and role of antibody affinity maturation. *Nat Commun* 11, 5413 (2020). [PubMed: 33110068]
65. Kang L et al. , A selective sweep in the Spike gene has driven SARS-CoV-2 human adaptation. *Cell* 184, 4392–4400 e4394 (2021). [PubMed: 34289344]
66. Harbison AM et al. , Fine-tuning the Spike: Role of the nature and topology of the glycan shield in the structure and dynamics of SARS-CoV-2 S. *bioRxiv*, 2021.2004.2001.438036 (2021).
67. Bloom JD, Gong LI, Baltimore D, Permissive secondary mutations enable the evolution of influenza oseltamivir resistance. *Science* 328, 1272–1275 (2010). [PubMed: 20522774]
68. Yurkovetskiy L et al. , Structural and functional analysis of the D614G SARS-CoV-2 spike protein variant. *Cell*, 739–751.e738 (2020). [PubMed: 32991842]
69. Kabsch W, Xds. *Acta Crystallogr D Biol Crystallogr* 66, 125–132 (2010). [PubMed: 20124692]
70. Evans PR, Murshudov GN, How good are my data and what is the resolution? *Acta Crystallogr D Biol Crystallogr* 69, 1204–1214 (2013). [PubMed: 23793146]
71. Bricogne G et al., BUSTER version 2.10.3, (Global Phasing Ltd., Cambridge, United Kingdom, 2017).
72. Emsley P, Lohkamp B, Scott WG, Cowtan K, Features and development of Coot. *Acta Crystallogr D Biol Crystallogr* 66, 486–501 (2010). [PubMed: 20383002]
73. Adams PD et al. , PHENIX: a comprehensive Python-based system for macromolecular structure solution. *Acta Crystallogr D Biol Crystallogr* 66, 213–221 (2010). [PubMed: 20124702]
74. Zheng SQ et al. , MotionCor2: anisotropic correction of beam-induced motion for improved cryo-electron microscopy. *Nat Methods* 14, 331–332 (2017). [PubMed: 28250466]
75. Rohou A, Grigorieff N, CTFFIND4: Fast and accurate defocus estimation from electron micrographs. *J Struct Biol* 192, 216–221 (2015). [PubMed: 26278980]
76. Wagner T et al. , SPHIRE-crYOLO is a fast and accurate fully automated particle picker for cryo-EM. *Commun Biol* 2, 218 (2019). [PubMed: 31240256]
77. Punjani A, Rubinstein JL, Fleet DJ, Brubaker MA, cryoSPARC: algorithms for rapid unsupervised cryo-EM structure determination. *Nat Methods* 14, 290–296 (2017). [PubMed: 28165473]
78. Walls AC et al. , Structure, function, and antigenicity of the SARS-CoV-2 spike glycoprotein. *Cell*, 281–292.e286 (2020). [PubMed: 32155444]
79. Zhang S et al. , Bat and pangolin coronavirus spike glycoprotein structures provide insights into SARS-CoV-2 evolution. *Nat Commun* 12, 1607 (2021). [PubMed: 33707453]
80. Xiao T et al. , A trimeric human angiotensin-converting enzyme 2 as an anti-SARS-CoV-2 agent. *Nat Struct Mol Biol* 28, 202–209 (2021). [PubMed: 33432247]
81. Harcourt J et al. , Severe Acute Respiratory Syndrome Coronavirus 2 from patient with coronavirus disease, United States. *Emerg Infect Dis* 26, 1266–1273 (2020). [PubMed: 32160149]
82. Aricescu AR, Lu W, Jones EY, A time- and cost-efficient system for high-level protein production in mammalian cells. *Acta Crystallogr D Biol Crystallogr* 62, 1243–1250 (2006). [PubMed: 17001101]
83. Hsieh CL et al. , Structure-based design of prefusion-stabilized SARS-CoV-2 spikes. *Science* 369, 1501–1505 (2020). [PubMed: 32703906]

84. Misasi J et al. , Structural and molecular basis for Ebola virus neutralization by protective human antibodies. *Science* 351, 1343–1346 (2016). [PubMed: 26917592]
85. Brochet X, Lefranc MP, Giudicelli V, IMGT/V-QUEST: the highly customized and integrated system for IG and TR standardized V-J and V-D-J sequence analysis. *Nucleic Acids Res* 36, W503–508 (2008). [PubMed: 18503082]
86. McCoy AJ et al. , Phaser crystallographic software. *J Appl Crystallogr* 40, 658–674 (2007). [PubMed: 19461840]
87. Jones TA, Zou JY, Cowan SW, Kjeldgaard M, Improved methods for building protein models in electron density maps and the location of errors in these models. *Acta Crystallogr A* 47 (Pt 2), 110–119 (1991). [PubMed: 2025413]
88. Williams CJ et al. , MolProbity: More and better reference data for improved all-atom structure validation. *Protein Sci* 27, 293–315 (2018). [PubMed: 29067766]
89. Pless DD, Lennarz WJ, Enzymatic conversion of proteins to glycoproteins. *Proc Natl Acad Sci U S A* 74, 134–138 (1977). [PubMed: 264667]
90. Watanabe Y, Allen JD, Wrapp D, McLellan JS, Crispin M, Site-specific glycan analysis of the SARS-CoV-2 spike. *Science* 369, 330–333 (2020). [PubMed: 32366695]
91. Zivanov J et al. , New tools for automated high-resolution cryo-EM structure determination in RELION-3. *Elife* 7, (2018).
92. Zhou T et al. , Cryo-EM structures of SARS-CoV-2 spike without and with ACE2 reveal a pH-dependent switch to mediate endosomal positioning of receptor-binding domains. *Cell Host Microbe* 28, 867–879 e865 (2020). [PubMed: 33271067]
93. Mitternacht S, FreeSASA: An open source C library for solvent accessible surface area calculations. *F1000Res* 5, 189 (2016). [PubMed: 26973785]
94. Lee B, Richards FM, The interpretation of protein structures: estimation of static accessibility. *J Mol Biol* 55, 379–400 (1971). [PubMed: 5551392]
95. Novotny J, Auffray C, A program for prediction of protein secondary structure from nucleotide sequence data: application to histocompatibility antigens. *Nucleic Acids Res* 12, 243–255 (1984). [PubMed: 6546418]
96. Pavlova A et al. , Machine learning reveals the critical interactions for SARS-CoV-2 spike protein binding to ACE2. *J Phys Chem Lett* 12, 5494–5502 (2021). [PubMed: 34086459]
97. Li F, Li W, Farzan M, Harrison SC, Structure of SARS coronavirus spike receptor-binding domain complexed with receptor. *Science* 309, 1864–1868 (2005). [PubMed: 16166518]
98. Mirdita M, Ovchinnikov S, Steinegger M, ColabFold - Making protein folding accessible to all. *bioRxiv*, 2021.2008.2015.456425 (2021).
99. Tortorici MA et al. , Ultrapotent human antibodies protect against SARS-CoV-2 challenge via multiple mechanisms. *Science* 370, 950–957 (2020). [PubMed: 32972994]
100. Ke Z et al. , Structures and distributions of SARS-CoV-2 spike proteins on intact virions. *Nature* 588, 498–502 (2020). [PubMed: 32805734]

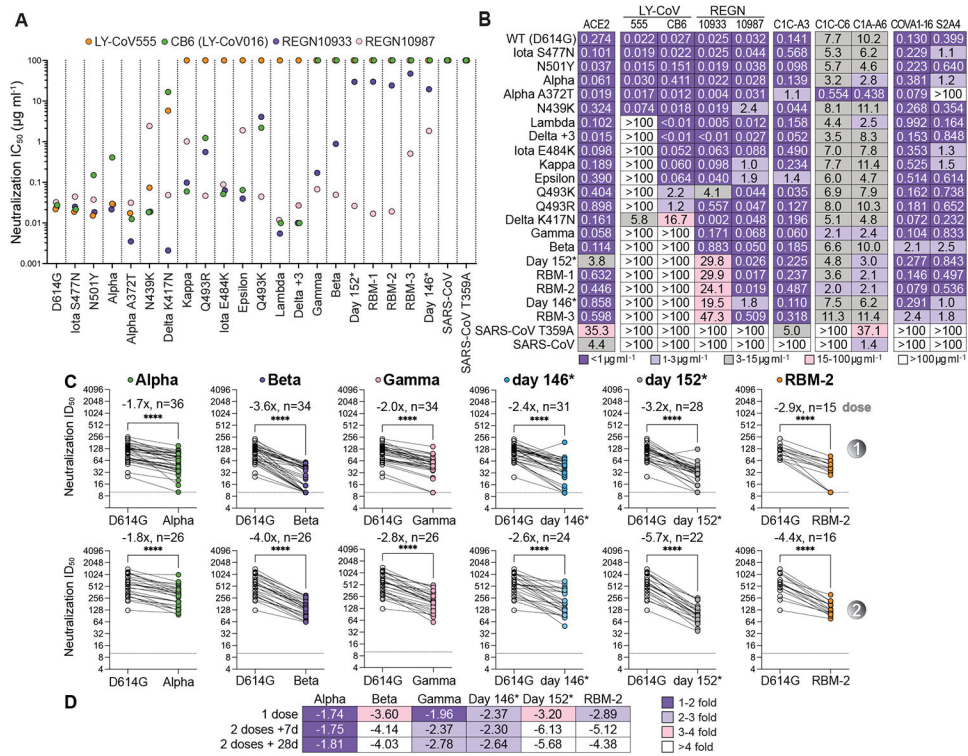


Fig. 2. Neutralization escape from therapeutic antibodies and mRNA vaccine-elicited serum. (A) Summary of neutralization IC₅₀ values for lentivirus pseudotypes with the indicated monoclonal antibodies. (B) Tabulated IC₅₀ values for lentivirus pseudotypes with the indicated monoclonal antibodies and an ACE2-Fc fusion protein (ACE2). (C) Mean ID₅₀ neutralization titers for the indicated variant pseudotypes at the time of the second immunization but prior to vaccination (“dose 1”), or twenty-eight days after second immunization (“dose 2”) with mRNA-1273 or BNT162b2. The fold change of the mean ID₅₀ neutralization titer with respect to D614G_S pseudotype is shown in each panel. Each experiment was performed twice independently in triplicate (*n*=6) (Wilcoxon matched-pairs signed rank test) (**** indicates *p*-value < 0.0001). (D) Tabulated fold change of mean ID₅₀ neutralization titers for the indicated pseudotypes as compared to D614G_S pseudotype.

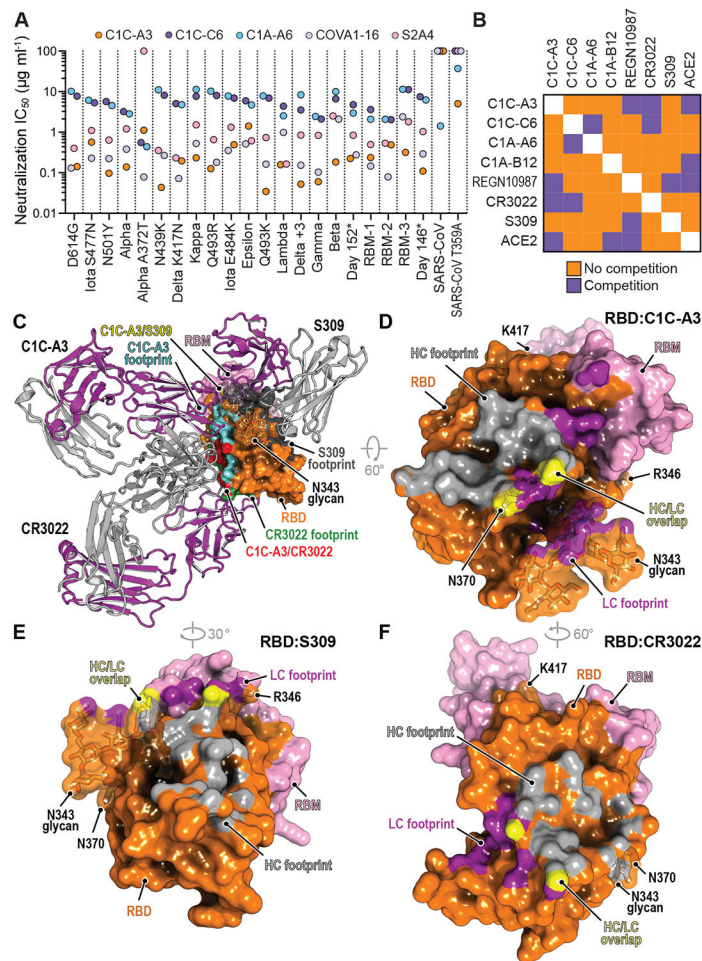


Fig. 3. Neutralization of SARS-CoV-2 variants by an RBD core targeting antibody. (A) Summary of neutralization IC_{50} values for pseudotypes and the indicated antibodies. (B) Summary of the results of biolayer interferometry-based competition assays. (C) Superposition of the CR3022 (PDB: 6W41) (55) and S309 (PDB: 6WPS) (44) structures onto the C1C-A3 bound RBD structure. Antibody Fabs are shown as ribbon diagrams and the RBD is shown in surface representation. Antibody footprints are shown on the RBD surface. (D) RBD footprint of C1C-A3. (E) RBD footprint of S309 (PDB: 6WPS) (44). (F) RBD footprint of CR3022 (PDB: 6W41) (55). In panels (D-F), key RBD residues discussed in the main text are highlighted.

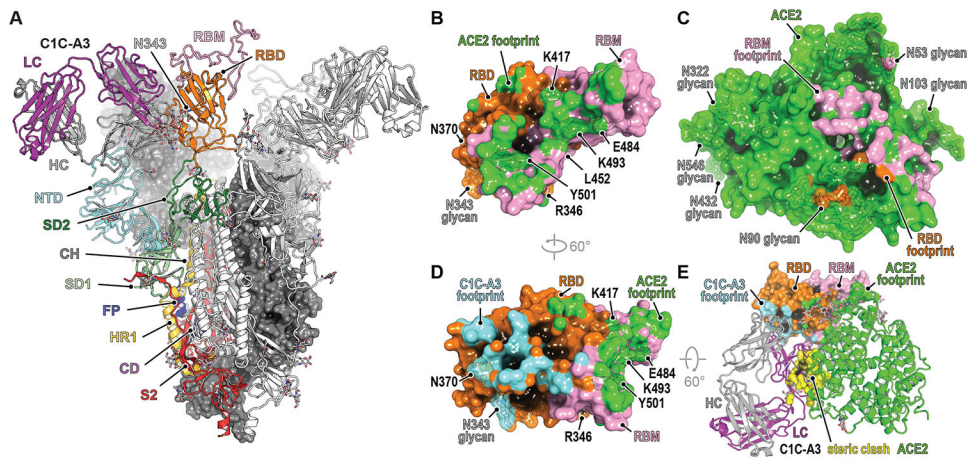


Fig. 4. Structural basis for C1C-A3 neutralization.

(A) cryo-EM structure of the C1C-A3 Fab SARS-CoV-2 spike protein complex. Two of the three spike protein protomers are shown in surface representation. One protomer is shown as a ribbon diagram with labeled subdomains. The trimer model shown was generated by superposition of an RBD-C1C-A3 Fab model generated by subparticle classification of the RBD region onto the coordinates of the trimeric spike protein-C1C-A3 Fab complex (see Materials and Methods). (B) Surface representation of the SARS-CoV-2 day 146* RBD showing the ACE2 footprint, including surfaces contacted by ACE2 N-linked glycans. Key RBD positions discussed in the text are labeled. (C) Surface representation of ACE2, showing the day 146* RBD and RBM footprints. (D) Surface representation of the RBD highlighting C1C-A3 Fab and ACE2 footprints. (E) Overlay of the C1C-A3 Fab:RBD complex with the day 146* RBD:ACE2 complex. Atoms within 1.54 Å of each other are shown in yellow surface representation to highlight steric clashes. Key RBD residues discussed in the text are labeled in panels (B) and (D).

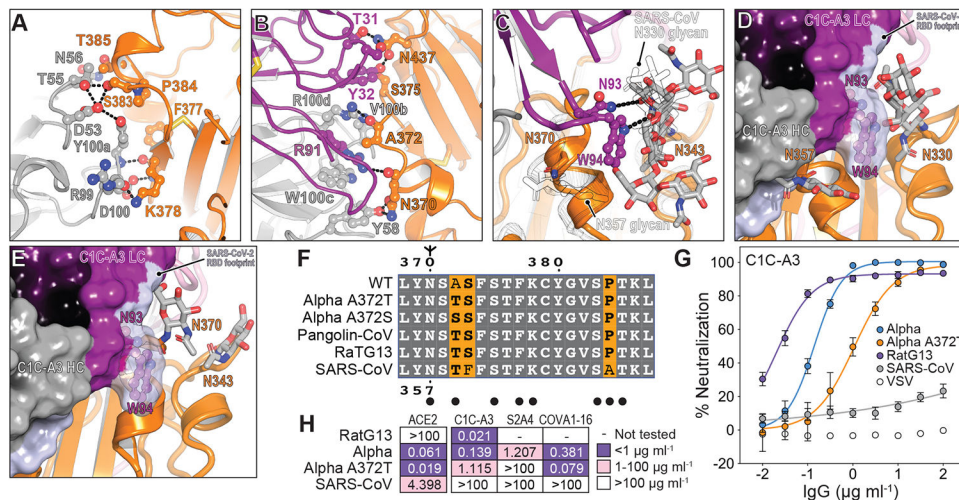


Fig. 5. Structural basis for immune evasion of a RBD core-targeting antibody.

(A and B) C1C-A3 antibody contacts with the SARS-CoV-2 RBD core. (C) C1C-A3 contacts with the N343_{RBD} glycan with structural superposition of the SARS-CoV RBD (PDB: 6NB6) (78). N-linked glycans found at N330_{RBD} and N357_{RBD} in SARS-CoV and the analogous N343_{RBD} and N370_{RBD} positions in SARS-CoV-2 are highlighted. (D) Superposition of the C1C-A3 Fab:SARS-CoV-2 RBD structure with the SARS-CoV RBD (PDB: 6NB6) (78) showing that a glycan attached at SARS-CoV N357_{RBD} may interfere with antibody binding. The SARS-CoV-2 RBD is not shown for clarity. (E) Superposition of the C1C-A3:SARS-CoV-2 RBD with the RaTG13 virus RBD (PDB: 7CN4) (79) showing that a glycan attached at RaTG13 virus N370_{RBD} would be more readily accommodated because the helix that contains it would be rotated away from the Fab. The SARS-CoV-2 RBD is omitted for clarity. (F) Sequence alignment of the RBD core region contacted by C1C-A3. SARS-CoV-2 numbering is shown at the top of the alignment, and SARS-CoV numbering is shown at the bottom. Circles indicate antibody contacts. (G) C1C-A3 neutralization curves for the indicated lentivirus pseudotypes. Data are plotted as the mean \pm standard deviation of the mean. The experiment was performed twice in triplicate ($n=6$). For some data points, error bars are smaller than symbols. (H) Tabulated neutralization IC_{50} values for the indicated pseudotypes.

Movie 1.

Author Manuscript

Author Manuscript

Author Manuscript

Author Manuscript